RSC Advances

ROYAL SOCIETY OF CHEMISTRY

www.rsc.org/advances

The effect of cerium alteration on the photocatalytic performance of WO_3 in sunlight exposure for water decontamination

M. Aslam[1], M. Tariq Qamar[1,2], M. Tahir Soomro[1], Iqbal M. I. Ismail[1,2], Z. A. Rehan[2,3], M. Waqar Ashraf[4], A. Hameed[1, 5*]

[1]Centre of Excellence in Environmental Studies (CEES), King Abdulaziz University, Jeddah 21589, Kingdom of Saudi Arabia.

[2]Chemistry Department, Faculty of Science, King Abdulaziz University, P.O. Box 80203, Jeddah 21589, Kingdom of Saudi Arabia.

[3]Centre of Excellence in Desalination Technology (CEDT), King Abdulaziz University, Jeddah 21589, Kingdom of Saudi Arabia.

[4]Department of Mathematics & Natural Sciences, Prince Mohammad Bin Fahd University, Al Khobar 31952, Saudi Arabia

[5]National Centre for Physics, Quaid-e-Azam University, Islamabad 44000, Pakistan.

[*]**Corresponding Author:**

Abdul Hameed, PhD

Centre of Excellence in Environmental Studies (CEES),

King Abdulaziz University, Jeddah 21589, Kingdom of Saudi Arabia

afmuhammad@kau.edu.sa, hameedch@yahoo.com

Abstract

In an effort to enhance the photocatalytic activity of cubic WO_3 in sunlight exposure, its surface was modified by impregnating the Ce^{3+} ions ranging from 1% to 20% with a step of 5% with respect to the weight of WO_3. Compared to pure WO_3, the optical analysis by diffuse reflectance spectroscopy (DRS) revealed better absorption cross-section and red shift in the band edges for Ce loaded catalysts. The decreased intensity of photoluminescence (PL) emissions and the suppression of the Raman active bands of WO_3 verified the recombination quenching ability of Ce surface states. The XRD analysis revealed the existence of Ce^{3+} states in the lower loadings ($\leq$ 5%), whereas the majority of Ce^{4+} states were noticed at higher loadings. The FESEM analysis also verified the formation of individual particles of Ce (III, IV) oxides at the surface of WO_3 at higher loadings. The XPS analysis of 10% Ce loaded samples also revealed the presence of mixed oxides of Ce at higher loading. Except for 1% Ce loaded WO_3, the estimation of charge-discharge capacity, in comparison to pure WO_3, revealed the enhancement in the charge retention ability with the increasing Ce loading. In comparison to pure WO_3, the synthesized catalysts exhibited superior activity for the removal of 2-nitrophenol and 2-chlorophenol substrates in natural sunlight exposure. The analysis of the degradation data revealed that in the lower concentration the surface oxygen bonded Ce^{3+} states serve as electron trapping and transfer centers, whereas with the increasing surface density the synergic composite mechanism is the dominating mode. The exaggerated estimation of Ce in the EDX analysis of the samples loaded with 15% and 20% Ce also revealed the major surface coverage by the oxides of Ce. The salient feature of the study was the evaluation of the photocatalytic activity with the minimal catalyst loading of 350 mg/L.

Keywords: Tungsten oxide, sunlight, cerium, degradation, mineralization

1. Introduction

The yellow tungsten trioxide (WO_3), because of its versatile physiochemical and optoelectronic properties, has received considerable prominence in the area of semiconductor photocatalysis.[1-3] The narrow band gap, low cost, non-toxic nature and high oxidation ability of the valence band holes marks WO_3 as a promising contender for visible or natural sunlight photocatalytic applications but unfortunately, because of the higher recombination rate of the excitons, WO_3 is rated as low efficiency photocatalyst.[4] Additionally, the potential of the excited conduction band electrons is not suitable enough to reduce the adsorbed oxygen (O_2) that severely affects the population of the potent reactive oxygen species (ROS) that is essential for the rapid degradation/mineralization of contaminants in environmental applications.[5-6] As WO_3 is responsive in the visible region of the solar spectrum, its suitable modification for higher photocatalytic activity can promote photocatalysis in natural daylight illumination and address the associated issues of high cost and technical complexity.[7-9] It is believed that the activity of WO_3 can be optimized for maximum efficacy by the alteration of its surface texture with metals and their respective oxides.[10-19]

The removal of hazardous chemical contaminants from the potable water especially is an essential prerequisite for consumption by living beings.[9, 20,21] A few articles have been reported so far for the degradation of phenols and its derivatives using either bare or modified WO_3 photocatalysts.[8, 22-24]

Being motivated by the excellent enhancement in the photocatalytic activity of ZnO after altering the surface with Ce^{3+} as surface modifier, the presented work is an effort to enhance the photocatalytic activity of WO_3 in natural sunlight exposure for environmental decontamination. [25, 26] The Ce metal ranging from 1% to 25 % with a step of 5% with respect to the weight of WO_3 was loaded by wet chemical impregnation method.[25-26] The synthesized catalysts were characterized by a variety of tools and their properties were compared with that of pure WO_3. The catalysts were subjected to electrochemical chronopotentiometry for the estimation of the probable role of surface Ce phases in enhancing the lifetime of excited states. The photocatalytic activity of cerium impregnated WO_3 was assessed for the degradation or mineralization of 2-NP and 2-CP

under natural sunlight irradiation. The effect of cerium loading on the surface WO_3 and the role of reactive oxygen species in the reaction mechanism was also assessed in the degradation or mineralization of phenols and its derivatives.

2. Experimental details

Tungsten oxide (WO_3) was synthesized by acidifying the solution of ammonium meta-tungstate. The low strength HNO_3 (0.05M) solution was added drop wise (15-20 drops/min) under constant stirring until pH ~3. Triton X-100 surfactant was used as surfactant to control the morphology of the synthesized powder. The complete precipitation was attained by heating the suspension at constant temperature of 150 ^oC for 2 h. The precipitates were washed several times with the (50:50) mixture of ethanol and Milli Q water for the removal of surfactant and excess HNO_3, dried in a hot air oven at 120 ^oC and finally calcined in a muffle furnace at 500 ^oC for 4 h. The 1%, 5%, 10%, 15%, 20% and 25% Ce^{3+} impregnated WO_3 catalysts were synthesized by impregnating the Ce^{3+} ions on the surface of the pre-synthesized WO_3. The amount of the Ce^{3+} ions was adjusted with respect to the weight of solid WO_3. In a representative synthesis, the precisely weighed amount of pre-synthesized WO_3 was added to the $Ce(NO_3)_3.6H_2O$ (Sigma-Aldrich) solution containing the appropriate quantity of Ce^{3+} ions. The suspension was aged overnight at room temperature under stirring. After drying the suspension at 100°C, the nitrates were decomposed at 200°C. The dried powder was calcined at 500°C for use in photocatalytic studies.

The solid-state absorption and diffuse reflectance spectra (DRS) of the synthesized Ce^{3+} coated WO_3 photocatalysts were acquired by Perkin Elmer UV-visible diffuse reflectance spectrophotometer in the 190-900 nm range. The Kubelka-Munk transformation, F(R), of %R data was used for the evaluation of the absorption edges of the synthesized powders. The photoluminescence (PL) emission spectra of the Ce^{3+} coated WO_3 powders were recorded by a fluorescence spectrometer, RF-5301 PC, Shimadzu, Japan, at an excitation wavelength of 325 nm, whereas the fluorescence emissions were recorded in 350 to 800 nm range. A DXR Raman Microscope, Thermo Scientific, USA, equipped with 532 nm laser as the excitation source at 6mW power was

employed to investigate the Raman shifts. The powder XRD patterns of bare and Ce^{3+} impregnated WO_3 powders were recorded by Xpert x-ray powder diffractometer (Philips PW1398) with Cu $K\alpha$ radiation source from 20^o to 80^o (2θ) with a step time of 3 seconds and step size of 0.05^o. The XPS analysis of 10% Ce loaded WO_3 powders were acquired by X-ray Photoelectron Spectrometer (PHI 5000 VersaProbe II, ULVAC-PHI Inc., USA) in 0–1100 eV binding energy range. The changes in the morphology of WO_3 base and the surface presence Ce^{3+} species were examined by Field Emission Scanning Electron Microscope (FEI, Quanta FEG 450, Quorum Q150R ES, Quorum Technologies Ltd. Ashford. Kent. England) at a voltage of 30kV whereas the coupled EDX accessory was used to estimate the percentage loading of Ce. A transmission electron microscope (JEOL ARM-200F, JEOL, Japan) was used for the microstructure analysis at an operating voltage of 200 kV.

The ability of Ce^{3+} coatings to retain the excited charge carriers was evaluated by chronopotentiometry (CP). A VSP multi-channel potentiostat (Bio-logic Science Instrument, USA) equipped with Ec-lab software in a three electrode system, namely; glassy carbon electrode (working electrode), platinum (counter electrode) and Ag/AgCl saturated electrode (reference electrode), was used to investigate the charge-discharge behavior of the synthesized powders in comparison to pure WO_3 in the neutral medium. The samples dispersed in chloroform were coated at a glassy carbon electrode by dropping 10µl of suspension and dried in hot air for film formation. The homogeneity of the film was analyzed optically. For acquiring charge-discharge measurements under illumination, a 50 watt halogen lamp was used as light source.

The experiments for the evaluation of the photocatalytic activity of pure and Ce^{3+} loaded WO_3 powders in sunlight exposure was performed by exposing 150 ml of 50 ppm of 2-nitrophenol (2-NP) and 2-chlorophenol (2-CP) solution containing 50 mg of respective catalyst. It is important to mention here that a minimum possible amount of the catalysts was used for degradation studies. All the experiments were performed with 350 mg/L catalyst loading under sunlight illumination of $1100\pm100 \times 10^2$ lx in the fixed period of the daylight. The 10 ml of the sample was drawn from the reactor after every 30 mins in the first two hours and 60 min in the last hour.

After removing the catalysts by 0.20µm Whatman disposable syringe filter, the collected sample was divided into two portions of 5ml each. One portion was used to measure the released ions by ion chromatography (IC) using Thermo scientific, USA, ion chromatograph, Dionex (ICS-5000 + EG Eluent Generator), whereas the second portion was subjected to high performance liquid chromatography (HPLC) HPLC, (SPD-20A, Shimadzu Corporation, Japan) and total organic carbon (TOC-VCPH, Shimadzu Corporation, Japan) analysis. The intermediates formed during the process were also identified using gas chromatography mass spectrometry (GC-MS, Shimadzu-QP2010 Plus, Shimadzu Corporation, Japan).

3. Results and Discussion

The comparison of the solid-state absorption spectra of pure and the synthesized Ce^{3+} loaded WO_3 photocatalysts is presented in Fig. 1a. The appearance of the smooth curve with the distinct absorption edge predicted the stoichiometric nature and well-defined crystal structure for pure WO_3.[8] In comparison to WO_3, an expansion in the absorption cross-section in the visible region (450-700 nm) was noticed for Ce^{3+} loaded WO_3 powders. The prime absorption in pure WO_3 is the bandgap excitation originated from the excitation of electrons from the valence band (O 2p) electrons to the conduction band (W 4f). The enhanced absorption by Ce^{3+} loaded samples in the visible region may be attributed to the transitions from O 2p to Ce ($4f^1 + 5d^o$) as Ce^{3+} ions share the singly charged surface oxygen to form W^{6+}-O-Ce^{3+} type structures at the surface of WO_3. Although the absorption of all the Ce^{3+} impregnated samples was higher than that of pure WO_3 however, a decreasing trend was noticed with the increasing surface density. This observation pointed towards the absorption of photons by the probable oxides of Ce that covers the surface of WO_3. The same is presented in the exploded view (inset of Fig. 1a). The graphical evaluation of the bandgaps of pure and synthesized Ce^{3+} impregnated catalysts is presented in Fig. 1b. For clarity, the plots of pure, 1% and 5% Ce^{3+} loaded WO_3 are presented in Fig. 1b, whereas that of 10%, 15%, 20% and 25% are presented in the inset of Fig. 1b. The evaluated bandgap of ~2.74 eV was in accordance with the literature values.[8, 16] The evaluated values of the direct band edge position, obtained by extrapolating the $(F(R) \times h\nu)^{1/2}$ versus photon energy ($h\nu$) curves to x-axis, were ~2.64

eV, ~2.61 eV, ~2.62 eV, ~2.65 eV, ~2.68 eV and ~2.73 eV, respectively. Additionally, the appearance of the single band edge for all the synthesized catalysts depicted homogeneous distribution of Ce^{3+} on the surface of WO_3. Although, compared to pure WO_3, a red shift in the band edge energies was observed for all the catalysts, however, beyond 5% Ce^{3+} loading a mild increase in the band edge positions was noticed. The unexpected variation in the bandgap energies with the increasing metal loading is explainable on the basis of the fact that at lower concentrations of Ce^{3+} the incoming Ce^{3+} ions bind with the singly charged surface oxygen to form surface Ce_2O_3 that results in the lowing of the bandgap of the impregnated material as the band edge position appear as the combined average effect of the bandgaps of Ce_2O_3 and WO_3. At higher concentrations, after the initial deposition of Ce^{3+} oxide layer, the deposition of the successive layers results the formation of CeO_2. Therefore, the bandgaps of the synthesized catalysts with Ce^{3+} loading beyond 5% appear as the combinatorial average effect of the bandgap energies of Ce_2O_3, CeO_2 and WO_3.

The comparison of the photoluminescence (PL) spectra of the pure and as-synthesized Ce^{3+} impregnated WO_3 photocatalysts is presented in the Fig. 2a. WO_3 is a photo-luminescent material and a broad emission band centered at 470 nm was observed on excitation at 325 nm in the PL spectra that corresponded to the radiative de-excitation from W^{6+} (4f) to O^{2-}(2p). The energy of the released emissions (~2.68 eV) was in sound agreement with the experimentally evaluated band edge position of 2.74 eV. The shoulders at 483 nm and 493 nm represent the emissions of the excited electrons trapped in the W^{5+} and O^{-} originated defects. The PL analysis is of particular importance in photocatalysis as it demonstrates the ability of the modifier for quenching the recombination of excited states. A gradual decrease in the PL intensity was noticed with the increasing Ce^{3+} contents at the surface of WO_3. Interestingly, the decrease in the intensity was not proportional with the Ce^{3+} loading. With respect to the intensity of the peak at 470 nm, a ~28%, ~43%, ~52%, ~58%, ~60% and ~56% decrease in the PL intensity was estimated for 1%, 5%, 10%, 15%, 20 and 25% Ce^{3+} loaded WO_3 catalysts, respectively.

The Raman spectra of the pure and as-synthesized Ce^{3+} impregnated WO_3 photocatalysts are compared in Fig. 2b. For pure WO_3 the major Raman peaks appeared at ~271.08 cm^{-1}, ~326.04 cm^{-1}, ~717.5 cm^{-1} and ~806.2 cm^{-1}. The bands centered at ~717.5 cm^{-1} and ~806.2 cm^{-1} were assigned to O-W-O stretching modes whereas the bands at 271.08 cm^{-1} and 326.04 cm^{-1} were originated by the bending of the bridging oxygen of W-O-W bonds.[27-28] The impregnation of Ce^{3+} significantly affected the intensity of the stretching modes of WO_3 that indicated the amplified stiffness of these band. The impregnating Ce^{3+} binds with the singly charged surface oxygen that resulted in the formation O-W-O-Ce type surface structures. It was interesting that the stretching modes were more affected as compared to the W-O-W bridging modes. The engagement of the surface oxygen, a major contributor in the stretching Raman active modes, by Ce^{3+} ions resulted in the decreased intensity. As presented in the inset of Fig 2b, the effect of the increasing Ce^{3+} surface loading on the position of the Raman active mode 806.2 cm^{-1} was evaluated by comparing the normalized bands for the pure and as-synthesized catalysts. Compared to pure WO_3 and for 1% to 15% loading, the peaks were shifted by ~1 cm^{-1} whereas for 20% and 25% Ce^{3+} loading, a shift of ~3 cm^{-1} towards higher energy was noticed.

The comparison of the XRD patterns of pure and as-synthesized Ce^{3+} impregnated WO_3 is presented in Fig. 3, where the dominance of the reflections arising from the base material, WO_3, and the appearance of the additional reflections, as marked by arrows, due to the corresponding oxides of Ce, is observable. Additionally, the decrease in the intensity of the reflections of WO_3 with the increasing Ce^{3+} contents was also noticed. For pure WO_3, the major reflections were matched with monoclinic WO_3 (JCPDS-43-1035). The detailed description regarding the corresponding *hkl* indices is presented in our previous communication.[16] The average evaluated crystallite size was 37.1 nm. Probably, due to the trivial changes in the synthetic procedure, a mild decrease in the crystallite size, compared to 45.2 nm in the previous study, was noticed.[16] The careful analysis of the XRD patterns revealed that the majority of the reflections originated due to the oxides species of Ce formed as a consequence of impregnation process were entrapped in the intense reflections of WO_3 however, the growth of some distinctive reflections was identified. These reflections were appeared at 2θ values of

~28.1, ~36.7 and ~39.3 degrees. The exploded view of the XRD patterns in the 2θ range of ~35.6º to ~40.6º, authenticating the existence/growth of the oxides of Ce, is presented in the inset of Fig. 3. During the effort to identify the phases, it was revealed that these reflection does not match to a single pattern rather matched with JCPDS # 44-1086 (hexagonal, Ce_2O_3) and JCPDS # 43-1002 (Cubic, CeO_2). Additionally, at lower Ce^{3+} loadings (up to 10%) the reflections due to impregnated Ce^{3+} were matched mostly with that of Ce_2O_3 whereas for higher concentrations (15%, 20% and 25% Ce^{3+} loaded WO_3) the reflections due to CeO_2 were prominent. These observations led to the interpretation that the oxidation state of Ce^{3+} changes to Ce^{4+} during the impregnation of higher Ce^{3+} concentrations.

The XPS survey scan of 10% Ce^{3+} loaded WO_3 is presented in Fig. 4a, where the peaks corresponding to the various components such as W, Ce and O are observable. The appearance of the peak of C1s at 285.08 eV validated the calibration. The individual high resolution scans of W4f, Ce3d and O1s core levels were recorded in the binding energy range of 25 to 43 eV, 880 to 925 eV and 524 to 536 eV range, respectively. The deconvoluted fitted peaks of W4f levels arising from WO_3 are presented in Fig. 4b. The appearance of splitted $W4f_{7/2}$ and $W4f_{5/2}$ levels at ~34.05 eV and ~37.1 eV identified tungsten in 6+ oxidation state. The observed values of the maxima's of the doublet of W4f were in accordance with the literature values for WO_3.[29] The fitted 3d splitted levels of 10% Ce^{3+} loaded WO_3 are presented in Fig. 4c. Although the Ce^{3+} was used in the synthesis, the deconvolution and fitting of the high resolution curve of Ce3d splitted levels revealed the co-existence of both Ce^{3+} and Ce^{4+} oxidation states in the sample. In the XPS analysis of pure CeO_2, the splitted $3d_{5/2}$ and $3d_{3/2}$ appear at ~887.58 eV and ~900.71 eV, whereas for Ce_2O_3 the same appear at ~892.78 eV and ~902.50 eV, respectively.[30] In the current study a mild variation in the position of the peaks is probably due to the presence of WO_3 in the matrix. The $3d_{3/2}$ peaks for Ce^{3+} and Ce^{4+} were appeared at ~902.5 eV and ~899.05 eV, respectively. The same was expected as Ce is highly susceptible to oxidation under even mild oxidizing conditions. The asymmetric O1s peak indicated also verified the existence of oxygen originated from the chemically different nature. The deconvolution and curve fitting of O1s core level is presented in Fig. 4d. The most intense peak at ~531.04 eV represented the oxygen attached to W^{6+}

species in the crystal structure, whereas the peaks at ~527.9 eV and ~523.5 eV represented the oxygen attached to Ce^{4+} and Ce^{3+}, respectively, that further verified the existence of Ce in III and IV oxidation states. The peak at ~533.8 eV was assigned to surface hydroxyl groups.

The comparison of the FESEM images of Ce^{3+} loaded samples with that of pure WO_3 at the magnification of 200,000× is presented in Fig. 5a-f, where the gradual deposition of Ce^{3+} at the surface in the form of respective oxides was evidenced. Compared to pure WO_3, the formation of additional phase composed of the oxides of cerium was evidenced for 5% and higher compositions. As per our previous experience, the presence of the Ce is also authenticated by the brightness of the FESEM images because of the accumulation of charge. The estimation of the amount of Ce loading was also performed by the coupled EDX analysis. The EDX spectra of pure, 5%, 10% and 20% Ce^{3+} loaded WO_3 are presented in Fig. 6, whereas the corresponding low resolution SEM images indicating the targeted positions as presented in the insets. Interestingly, only the estimated W% values of the loaded Ce metal for 5% (4.66%) and 10 % (9.38%) samples were in close agreement with the experimental values whereas, significantly low value of 0.4% for 1% and substantially high values of 28% and 51% were observed for 15% and 20% Ce^{3+} loaded samples. The further verification of the percentage of the Ce loading in comparison to the actual amount used was carried out by ICP-OES analysis by dissolving the loaded Ce in nitric acid as WO_3 is insoluble in acids. The evaluated values were in satisfactory agreement with the actual amount used for surface modification. As EDX estimates the composition of the surface, probably, 1% Ce^{3+} loading is low enough for the precise estimation that resulted in the low values. Similarly, at higher Ce^{3+} loadings, i.e. 15%, 20% and 25%, it seems that the majority of WO_3 surface is covered by the oxides of the loaded Ce. The major portion of the incident electron beam interacts with the oxides of cerium rather than WO_3 thus detecting Ce as major component at the surface.

A typical HRTEM micrograph of 5% Ce loaded sample is presented in Fig. 7a where the base material (WO_3) and the loaded Ce (III, IV) oxide fine nanoparticles are apparent. The particle size ~55.25 nm of the focused WO_3 particle was in accordance

with the average crystallite size of ~37.1 nm by XRD analysis. The loaded Ce (III, IV) oxide particles appeared as aggregates of the smaller particle with the size ranges between 4-21 nm. Fig. 7b shows the further magnification of the image presented in Fig. 7a where the microstructures of the single crystals of WO_3 (marked by orange dotted circle) and Ce (III, IV) oxide (marked by red dotted circle) are evident. The HRTEM images of single crystals isolated in the red and orange marked areas of Fig. 7a are presented in Fig. 7c and d, respectively, where in both the crystal types, excellent homogeneity and well defined structural alignment, depicting the high crystallinity, is observable. The corresponding line scans are presented in Fig. 7e and f. The observed d spacing of 0.33 nm and 0.35 nm were in accordance with the literature values for cubic CeO_2 and monoclinic WO_3, respectively.[31,32]

The galvanostatic charge-discharge behavior of pure, 1%, 5%, 10%, 15%, 20% and 25% Ce^{3+} modified WO_3 was evaluated both in the dark and under illumination at a current density of 0.1 A/m^2 in cathodic and anodic directions. The plots of E(V) versus the time (s) for pure WO_3 and Ce^{3+} loaded catalysts are presented in Fig. 8a-f. Considering sufficiently longer period for the completion of oxidation and reduction reactions, all the measurements were recorded for 180s. All the powders including bare WO_3 exhibited pseudo-capacitive characteristics (non-ideal triangular behavior), in the dark as well as under illumination, illustrating near absence of electrochemical double layer characteristics. It is a well-established fact about photochromic WO_3[8,16,33] that under illumination, as a consequence of UV photon interaction, labile oxygen is released from the surface generating W^{5+} based defects or vacancies that serve as traps for excited electrons. Fig. 8a shows CP curves of the three cycles of the pure WO_3 in the dark and under illumination. Each cycle was recorded after a period of five mins in the both conditions. It is interesting to notice that the discharge capacity (charge retaining capacity) gradually increases in each cycle attributing to the progressive generation of W^{5+} vacancies with increasing exposure time. A decrease in discharge capacity was witnessed for 1%Ce^{3+} loaded WO_3 (Fig. 8b), depicted the suppression of the process of formation of W^{5+} states that resulted in the decreased charge retaining ability of the material. Compared to pure WO_3, a mild increase in discharge capacity was noticed for 5% Ce^{3+} (Fig. 7c) loaded powder under illumination. The transfer of the excited

conduction band electrons from W4f to closely spaced Ce ($4f^1$ + $5d^o$) is the plausible argument in this context. A successive increase in the discharge capacity was noticed with the increasing Ce^{3+} loading however, compared to 20% no significant change was noticed for 25% Ce^{3+} loaded sample (Fig. 8d-f). The formation of the oxides of Ce^{3+} and Ce^{4+} that serve as the traps for the excited electrons (e^-) and photogenerated holes (h^+) and the mutual transfer of charges between Ce^{3+} and Ce^{4+} states generated as a result of the direct absorption of photons by the oxides of loaded metal are the probable sources of enhanced retention.

In the photocatalytic degradation process, the efficiency of a photocatalysts is based on its ability to utilize the photon generated charge carriers in the generation of the oxidizing radicals such as superoxide anion and hydroxyl radicals. The population of these species in a photocatalytic system estimates the effectiveness of a photocatalyst in transferring the charge carriers to the adsorbed oxygen and water molecules as given below.

$$(O_2)_{ads} + e^-_{cb} \rightarrow O_2^{\bullet -} \qquad (1)$$

$$H_2O + h^+_{vb} \rightarrow H_2O^+ \rightarrow HO^{\bullet} + H^+ \qquad (2)$$

In the aqueous medium, the charge transfer ability of the semiconductor and the simultaneous formation of superoxide anion ($O_2^{\bullet -}$) and hydroxyl radicals ($HO^{\bullet}$) is entirely dependent on the potential of the conduction and valence band edge, respectively. Additionally, some other factors such as pH of the system and pH_{ZPC} also contribute in this regard.

The comparison of the time-scale UV-visible degradation profiles of 2-NP over pure and 20% Ce^{3+} loaded WO_3 in sunlight exposure are presented in the Fig. S1a† and b† (Electronic supplementary information), respectively, where compared to pure WO_3 an efficient degradation of 2-NP was observable on 20% Ce^{3+} loaded WO_3. In the UV-visible absorption spectra of 2-NP, two distinct absorption maxima appear at 279.5 nm and 349.5 nm. As per our observation, during the degradation process, the decrease in the intensity of both the peaks was proportional, therefore, the percentage degradation of 2-NP as a function of illumination time was evaluated on the basis of the decrease in the

intensity if the peak at 349.5 nm. The comparison of the percentage degradation of 2-NP, as a function of sunlight exposure time, over pure, 1%, 5%, 10%, 15%, 20% and 25% Ce^{3+} loaded WO_3 is presented in Fig. 9a. Although higher or comparable with pure WO_3, an irregular behavior of the catalysts was noticed with the increasing surface loading of Ce^{3+}. Compared to pure WO_3, a mild increase in the degradation activity was noticed for 1% Ce^{3+} loading whereas, the degradation process was significantly escalated for 5% loading. With the further increase in the metal loading i.e. for 10% Ce^{3+} loaded WO_3, the degradation process was decelerated with higher activity than bare and 1% Ce^{3+} loaded WO_3 but significantly lower than 5% Ce^{3+} loading. Beyond 10% Ce^{3+} loading, a successive increase in the degradation activity was witnessed with the increasing metal loading of 15% and 20% loaded samples. Interestingly, the activity of both the catalysts was even higher than 5% Ce^{3+} loaded WO_3. Compared to ~19% degradation for pure WO_3, in the initial 30 min of the sunlight exposure, ~24%, ~44%, ~34%, ~47%, ~57% and ~47% of 2-NP was degraded over 1%, 5%, 10%, 15%, 20% and 25% Ce^{3+} loaded WO_3, respectively. Although, all the catalysts, including pure WO_3 managed to degrade ≥90% of 2-NP in 300 min of sunlight exposure however, the complete removal i.e. >99.5% was experiential for 5%, 15% and 20% Ce^{3+} loaded WO_3. The evaluation of the rate constants "k" for the degradation process over pure and as-synthesized Ce^{3+} impregnated WO_3, obtained by plotting $\ln(C_o/C)$ versus the sunlight exposure time, is presented in Fig. 9b. The rate constants of 0.0082 min^{-1}, 0.0096 min^{-1}, 0.012 min^{-1}, 0.013 min^{-1} and 0.015 min^{-1} and 0.018 min^{-1} were evaluated for pure, 1%, 5%, 10%, 15% and 20% Ce^{3+} loaded WO_3, respectively. For 25% Ce^{3+} loaded catalyst, a linear rate of degradation in 180 mins of exposure followed by a sharp increase afterwards. The observed was consistent with our previous study with pure CeO_2[30] and suggested the majority surface coverage by the oxides of Ce (III, IV).

The degradation of 2-CP was evaluated on the basis of the time-scale decrease in the peak heights of the substrate in the HPLC analysis with the progress of the reaction. For illustration, the comparison of the HPLC degradation profiles of 2-CP over pure and 20% Ce^{3+} impregnated WO_3 is presented in the electronic supplementary information of Fig. S1c† and d†, where a successive decrease of 2-CP substrate and formation as well as removal of the intermediates with the increasing exposure time is observable. The

percentage degradation profile for the degradation of 2-CP in the presence of each catalyst, extracted from the decrease in the peak heights, is presented in Fig. 9c. For all the catalysts, in the initial 30 min of sunlight exposure, the degradation pattern of 2-CP was comparable with that of 2-NP and a degradation of ~18%, ~29%, ~35%, ~38%, ~45%, 50% and ~46% over pure, 1%, 5%, 10%, 15%, 20% and 25% Ce^{3+} loaded WO_3, respectively. A significant increase in the percentage degradation was witnessed with the progress of the reaction and all the catalysts, including WO_3 managed to degrade ≥90% of 2-CP in 180 min of sunlight exposure. Except for pure and 1% Ce^{3+} loaded WO_3, all the catalysts completely (≥99.5%) removed 2-CP in 300 min of sunlight exposure. The graphical evaluation of the rate constants for the degradation of 2-CP over pure and as-synthesized WO_3 catalysts is presented in Fig. 9d. The observed rate constants were 0.012 min^{-1}, 0.013 min^{-1}, 0.018 min^{-1}, 0.015 min^{-1}, 0.020 min^{-1} and 0.022 min^{-1} for pure, 1%, 5%, 10%, 15% and 20% Ce^{3+} loaded WO_3, respectively. The observation regarding the variations in the rate of degradation of 2-CP over 25% Ce^{3+} loaded catalyst were similar to that already explained for 2-NP.

The mineralization of 2-NP and 2-CP over pure and as-synthesized Ce^{3+} loaded WO_3 photocatalysts was evaluated by measuring the TOC removal during the course of the degradation process and the comparison of the percentage TOC removal for both the substrates is presented in Fig. 10a and b. In the initial 30 min of the exposure, the TOC removal for both the substrates was significantly lower than the degradation of substrates. For 2-NP, a TOC removal ≥15% was witnesses for 5%, 15%, 20% and 25% Ce^{3+} impregnated WO_3, whereas for pure WO_3, 1% and 10% Ce^{3+} loaded catalysts, it was lower than 10%. A similar trend prevailed for 2-CP however, the TOC removal was less than ~15% for 5%, 15%, 20% and 25% Ce^{3+} impregnated WO_3. In the 300 mins of exposure, ~92% and ~86% mineralization of 2-NP and 2-CP, respectively, was observable over 20% Ce^{3+} loaded WO_3 catalyst. The evaluation of the rates of mineralization of 2-NP and 2-CP are presented in the Fig. S2a† and b†, respectively. Interestingly, contrary to degradation process, the rates of mineralization of 2-NP on pure and as-synthesized catalysts were higher than that of 2-CP.

Tungsten oxide (WO_3) is an n-type semiconductor with a bandgap, depending on the morphology and particle size, ranging between 2.6-2.8 eV. In the aqueous medium, it

possesses the valence and conduction band edges at +3.44V and +0.74V, respectively. The significantly higher positive potential of the conduction band edge explicitly predicts the inability of WO_3 for the generation of superoxide anion radicals ($O_2^{\bullet-}$) (Eqn. 1) whereas, the sufficient potential of the valence band edge supports the formation of hydroxyl radicals ($HO^{\bullet}$) via water oxidation (Eqn. 2). In the results presented above, the rapid degradation and mineralization of the substrates (2-NP and 2-CP) substantiate the involvement of the superoxide anions in the degradation process. Although the potential of the band edges of the semiconductor is an important parameter in predicting the nature and population of the probable reactive oxygen species produced in aqueous system under illumination, however, there are certain additional factors that play a vital role in promoting the yield of ROS. For bare WO_3, the W^{5+} based defects in the vicinity of the conduction band, serve as excited electrons trap and transfer centers for the generation of superoxide radicals.[8,16,24] Additionally the population of these defects is further escalated under illumination. As compared to pure WO_3, the enhanced activity of 5% Ce^{3+} modified WO_3 indicate the supporting role of the Ce^{3+} surface states in suppressing the non-prolific recombination process. The potential of surface Ce^{3+} states in suppressing the recombination process is also validated by the decreased luminescence intensity in PL analysis (Fig. 2a). It seems quite logical that the placement of Ce^{3+} at the surface of WO_3 adds the additional defects to the already existing W^{5+} defects that serve as the electron trap and transfer centers for the generation of reduced oxidizing species such as $O_2^{\bullet-}$ radicals. The excited electrons from the conduction band of WO_3 are transferred to either W^{5+} states or Ce^{3+} states present in the vicinity. The other possible proposition is the direct transfer of the excited electrons from the valence band of WO_3 (O2p) to the empty valence shell of Ce^{3+} (5d + 4f) as the possible sites of attachment for the incoming Ce^{3+} entities is the singly charged surface oxygen (surface-O^-). The same may be represented pictorially as below in scheme I.

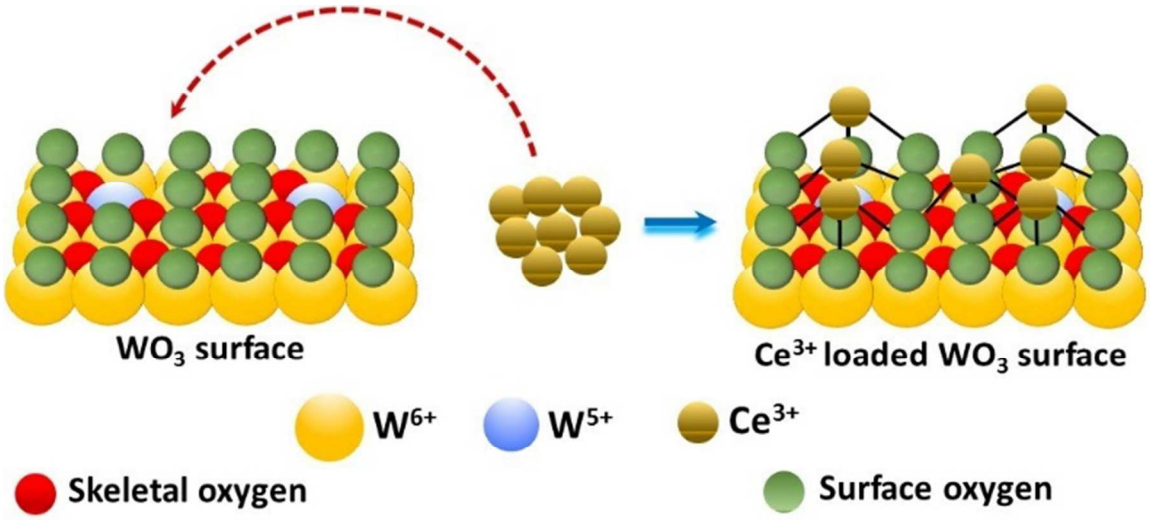

Scheme I: The process of binding of Ce^{3+} ions with the surface oxygen of WO_3.

Contrary to what we observed for the impregnation of Ce^{3+} on the hexagonal ZnO,[25,26] where we noticed the layer by layer deposition of Ce^{3+} in the form of respective oxides, in case of impregnation on WO_3, instead of layered deposition, the formation of the individual particles, with varying morphology of respective oxides was observable at

the higher Ce^{3+} loading. The same was evidenced in the FESEM analysis of the Ce^{3+} loaded samples (Fig. 5). The formation of the individual particles of Ce^{3+} and Ce^{4+} oxides at the surface of WO_3 leads to the composite nature of the catalysts and the mode of suppressing the charge carrier's recombination process and the delivery of the excited electrons to the reductants is entirely changed. Additionally, the surface Ce (III, IV) oxides being semiconductor in nature behave as independent photocatalysts with the absorption of a fraction of the incident photons. The fraction increases with the increase in the surface density of the oxide particles. As observed in our previous studies,[7] the formation of the composite photocatalysts is characterized by the appearance of the individual absorption edge of the components in the solid-state absorption or diffuse reflectance spectroscopy. In the current study, the same was not evidenced due to minor differences in the bandgaps of the components involved, however, the shifting of the absorption edges towards higher energy with the increasing Ce^{3+} loading (Fig. 1b) favors the above mentioned reasons. The mild increase in the photocatalytic activity for 1% Ce^{3+} loaded WO_3 catalyst depicted that probably the population of impregnated Ce^{3+} states is not sufficient enough to bring about any visible change rather suppress the formation of W^{5+} states. The same was also conceived from charge-discharge evaluation (Fig. 8). The increased concentration of Ce^{3+} states as evidenced for 5% Ce^{3+} loaded sample, effectively transfer the trapped electrons that results in the enhanced activity. The decreased emission intensity in the PL analysis supports the charge recombination quenching capability of the surface Ce (III, IV) Oxides. Based on the XRD analysis, the surface oxide layer may be considered as the mixture of CeO_2 and Ce_2O_3 with CeO_2 in excess at the higher metallic loadings. The band edge potentials of the valence and the conduction band of CeO_2 versus the NHE are +2.65 V and −0.53 V, whereas for Ce_2O_3 at +1.9 V and -0.50 V, respectively.[26,30] With the absorption of photons by WO_3 with the band edge positions at +3.44V and +0.74V, based on the electrochemical consideration, the transfer of photogenerated holes from the valence band of WO_3 to that of CeO_2 or Ce_2O_3 can be regarded as a most favorable process. This process may enhance the generation of ROS associated with the oxidation of water, however, the formation of superoxide anions will be drastically affected due to the potential (+0.74 V) associated with the conduction band of WO_3 that results in the decreased degradation of substrates.

Additionally, the presence of CeO_2 particles affects the transfer of electrons trapped in W^{5+} or Ce^{3+} defects to the reductants. The above discussion is summarized in scheme II.

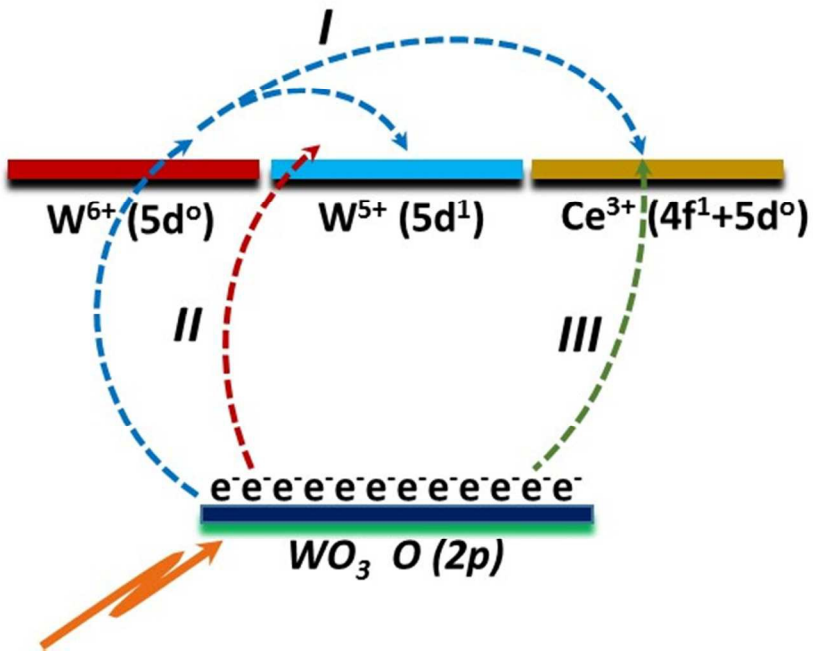

Scheme II: The probable transition routes of excited electrons when the light is absorbed by WO_3.

With the further increase in the surface loading i.e. from 10% Ce^{3+} loading, the fraction of the absorbed photons by the CeO_2 or Ce_2O_3 particles is increased, whereas due

to the surface coverage the contribution from WO_3 is reduced that affect the activity drastically. In this case, both the components independently absorb photons, facilitate each other in enhancing the lifetime of the excited states by the mutual transfer of photogenerated carriers. In the current case, as the fraction of the photons absorbed by WO_3 is reduced, whereas that by the surface oxides of Ce (III, IV) is increased, the excited electrons before being transferred to the adsorbed/dissolved oxygen are transferred to the conduction band of WO_3 by energetically allowed process that results in the reduced generation of ROS. The consistently increased activity of the Ce^{3+} impregnated catalysts indicated the major contribution of Ce^{3+}/Ce^{4+} oxides in the photocatalytic process. With the increase in surface loading, the fraction of the incident photons absorbed by the Ce^{3+}/Ce^{4+} oxides compared to the WO_3 base is significantly augmented. In this situation with the improved surface coverage, the activity of WO_3 support is overshadowed by that of surface Ce^{3+}/Ce^{4+} oxides. The suitability of band edges of cerium (Ce^{3+}/Ce^{4+}) oxides for the generation of ROS is already discussed above in detail. The enhanced degradation as well as mineralization of phenolic substrates over 15% and 20% Ce^{3+} impregnated WO_3 catalysts also supports the same. The selected samples, drawn after initial 30 min of sunlight exposure for each substrate, were further analyzed by GC-MS to identify the intermediates generated during the degradation process. It was noticed that the majority of the intermediates were aliphatic oxygenates. For both the substrate (2-CP and 2-NP) some common products such as CH_3COOH, CH_3COOCH_3, $C_3H_6O_3$ etc. were also identified. The further interaction of ROS with the intermediates leads to the formation of smaller fragments initially and later to CO_2 in successive interactions.[34]

The measurement of the released ion during the degradation process can provide a deep insight of the nature and mechanism of action of ROS involved in the degradation process. The representative IC profiles of the anions released during the degradation of 2-NP over 20% Ce^{3+} impregnated WO_3 are presented in Fig. 11a whereas, the comparison with that of pure and 5% Ce^{3+} loaded WO_3 catalysts is presented Fig. S3† (Supplementary Information). The release of anions i.e. NO_2^- and NO_3^-, over pure WO_3, in the current study was consistent with the already reported for the disc shaped WO_3.[8] The minor variation in the results is probably due to the changed morphology. It is important to

mention here that due to the change in instrumental parameters for better resolution because of the low concentration of ions, a mild shift in the retention time was noticed that was verified by comparing the results with standards. Compared to the expected theoretical value, a lower concentration of NO_2^- and NO_3^- ions was observed in the solution. As given in the Eqn. 3 below, the only explanation of this effect is the escape of nitrite ions as NO_2 gas from the solution after interaction with the photogenerated holes.[8]

$$NO_2^- + h^+ \rightarrow NO_2 \uparrow \qquad (3)$$

The formation of NO_2 gas as proposed above, is not a single step process rather involves the formation of a variety of radical and anionic species including NO_3^- ions. An alternative mechanism for the formation of NO_3^- ions can be proposed as follows;

$$NO_2^- + h^+ \rightarrow NO_2^{\bullet} \qquad (4)$$

$$NO_2^{\bullet} + O_2^{\bullet -} \rightarrow NO^- + O_2 \qquad (5)$$

$$NO^- + h^+ \rightarrow NO^{\bullet} \qquad (6)$$

$$NO^{\bullet} + O_2^{\bullet -} \rightarrow NO_3^- \qquad (7)$$

The representative IC profiles for the released ions during the degradation of 2-CP over 20% Ce^{3+} loaded WO_3 are presented in Fig. 11b whereas, the comparison with that of pure and 5% Ce^{3+} loaded WO_3 catalysts is presented Fig. S3† (Supplementary Information). The presence of minor peaks in the IC profiles also supports the above proposed mechanism. For 5% Ce^{3+} impregnated WO_3, the concentration of NO_2^- was significantly higher than that of pure WO_3, however, lower than the theoretical values. Additionally, a higher conversion of NO_2^- to NO_3^- ions led to the inference that the increased population of ROS, especially superoxide anion radicals, with 5% Ce^{3+} loading, initiates further interaction with the released NO_2^- ions, as proposed above, leading to the formation of NO_3^- ions. A consistent increase in the concentration of NO_2^- and NO_3^- for 20% Ce^{3+} loaded WO_3 revealed the enhanced formation of ROS. For 20% Ce^{3+} loaded WO_3, as detailed above, due to the extended surface coverage, the major fraction of incident photons is absorbed by the Ce^{3+}/Ce^{4+} oxide species, a changed mode of

interaction of ionic species with the photon generated reactive sites is also expected that results in the lower conversion of NO_2^- to NO_2 gas. The vital role of the potential of the valence band edge cannot be ignored in this regard. Besides Cl^-, the other anions identified were ClO_2^-, ClO_3^- and ClO_4^-. These ions were identified by analyzing the respective salt solutions under similar experimental conditions. Similar to that for 2-NP, the existence of these ions as mineralization products revealed the interaction of the initially released Cl^- with the ROS and photon generated reactive sites such as photogenerated holes (h^+).

The reusability of the 20% Ce^{3+} impregnated WO_3 was estimated in five consecutive cycles using the fresh 2-CP and 2-NP solution each time for the same catalyst. The catalyst showed sustained activity with acceptable variations in the activity. The graphical presentation of the reusability of the catalyst is presented in Fig. 12.

The other useful information that was extractable from the comparison of the IC profiles is regarding the population, nature and mode of interaction of the ROS generated or involved in the degradation as well as mineralization process. The variations in the yield of anions with different catalysts, in combination with the degradation and TOC profiles, depicts the ROS generation ability of the respective catalysts whereas the presence of respective anions i.e. NO_2^- and Cl^- ions for 2-NP and 2-CP, from the beginning of the exposure demonstrate the displacement of theses ions by the ionic ROS (superoxide anion) for the initiation of the degradation process. Additionally, the insertion of superoxide anions in the carbon chain provides the secondary stream of reactive sites that facilitates mineralization.

4. Conclusions

The impregnation of Ce^{3+} enhances the photocatalytic activity of WO_3 in sunlight exposure. At lower loadings, Ce^{3+} binds with the surface oxygen of WO_3 and generate additional defect sites along with the inherent W^{5+} defect states that serve as trap and transfer centers for the excited electrons. The XRD analysis revealed the Ce^{4+} oxides along with Ce^{3+} oxides whereas FESEM imaging revealed the formation of the particles of respective oxides at moderate and higher Ce^{3+} loading. For 10% Ce^{3+} loading, with the

increase in the absorption of the fraction of incident photons, the activity is reduced by the mutual transfer of charge carriers between Ce^{3+}/Ce^{4+} oxides and WO_3 whereas for loadings higher than 10%, with extended surface coverage, Ce^{3+}/Ce^{4+} oxides are the majority contributors in the photocatalytic degradation/mineralization. The NO_2 and Cl groups in 2-NP and 2-CP are released in the solution after being displaced by superoxide anion radicals. The released ions further interact with the active sites and ROS in the system.

Acknowledgements

Authors are thankful to the Center of Excellence in Environmental Studies (CEES), King Abdulaziz University and Ministry of Higher Education (MoHE), Kingdom of Saudi Arabia, for their supports.

References

1 L. Yin, D. Chen, M. Feng, L. Ge, D. Yang, Z. Song, B. Fan, R. Zhang and G. Shao, *RSC Adv.,* 2015, **5,** 328–337.

2 G. Wang, Y. Ling, H. Wang, X. Yang, C. Wang, J. Z. Zhang and Y. Li, *Energy Environ. Sci.*, 2012, **5**, 6180–6187.

3 Z. Meng, A. Fujii, T. Hashishin, N. Wada, T. Sanada, J. Tamaki, K. Kojima, H. Haneoka and T. Suzuki, *J. Mater. Chem. C* 2015, **3**, 1134–1141.

4 L. V. C. Lima, M. Rodriguez, V. A. A. Freitas, T. E. Souza, A. E. H. Machado, A. O. T. Patrocínio, J. D. Fabris, L. C. A. Oliveira and M. C. Pereira, *Appl. Catal. B* 2015, **165,** 579–588.

5 J. Zhang and Y. Nosaka*, J. Photochem. Photobiol. A: Chem.,* 2015, **303,** 53–58.

6 F. Amano, E. Ishinaga and A. Yamakata, *J. Phys. Chem., C*, 2013, **117**, 22584-22590.

7 M. Aslam, I. M. I. Ismail, T. Almeelbi, S. Chandrasekaran and A. Hameed, *Chemosphere*, 2014, **117C**, 115-123.

8 M. Aslam, I. M. I. Ismail, S. Chandrasekaran and A. Hameed, *J. Hazard. Mater.*, 2014, **276**, 120-128.

9 S. Ahmed, M. G. Rasul, R. Brown and M. A. Hashib, *J. Environ. Manag.*, 2011, **92**, 311-330.

10 I. Aslam, C. Cao, M. Tanveer, M. H. Farooq, W. S. Khan, M. Tahir, F. Idrees and S. Khalid, *RSC Adv., 2*015, **5,** 6019–6026.

11 M. K. Aminian and M. Hakimi, *Catal. Sci. Technol.,* 2014, **4,** 657–664.

12 J. Liu, S. Han, J. Li and J. Lin, *RSC Adv.,* 2014, **4,** 37556–37562.

13 S. Bai, K. Zhang, J. Sun, R. Luo, D. Li and A. Chen, *CrystEngComm*, 2014, **16**, 3289–3295.

14 S. Adhikari, D. Sarkar and G. Madras, *RSC Adv.,* 2015, **5,** 11895–11904.

15 W. Mu, X. Xie, X. Li, R. Zhang, Q. Yu, K. Lv, H. Wei and Y. Jian, *RSC Adv.,* 2014, **4,** 36064–36070.

16 A. Hameed, M. Aslam, I. M. I. Ismail and M. A. Gondal, *Appl. Catal. A*, 2014, **470**, 327-335.

17 S. A. Singh and Giridhar Madras, *Sep. Purif. Technol.,* 2013, **105,** 79–89.

18 K. Jothivenkatachalam, S. Prabhu, A. Nithya and K. Jeganathan, *RSC Adv.,* 2014, **4,** 21221–21229.

19 S. F. Chen, Y. F. Hu, S. G. Meng and X. L. Fu, *Appl. Catal., B*, 2014, **150–151**, 564–573.

20 S. Rasalingam, H. S. Kibombo, C. M. Wu, R. Peng, J. Baltrusaitis and R. T. Koodali, *Appl. Catal., B*, 2014, **148-149**, 394–405.

21 Z. Guo, R. Ma and G. Li, *Chem. Eng. J.*, 2006, **119**, 55–59.

22 C. F. Lin, C. H. Wu and Z. N. Onn, *J. Hazard. Mater.*, 2008, **154**, 1033–1039.

23 M. Zhang, C. Yang, W. Pu, Y. Tan, J. Zhang and K. Yang, *Electrochim. Acta,* 2014, **148**, 180–186.

24 A. Hameed, M. Aslam, I. M. I. Ismail, S. Chandrasekaran, M. Kadi and M. A. Gondal, *Appl. Catal., B*, 2014, **160-161**, 227-239.

25 I. M. I. Ismail, M. Aslam, T. Almeelbi, S. Chandrasekaran and A. Hameed, *RSC Adv.,* 2014, **4**, 16043-16046.

26 M. Aslam, I. M. I. Ismail, S. Chandrasekaran, T. Almeelbi and A. Hameed, *RSC Adv.,* 2014, **4,** 49347-49359.

27 R. F. Garcia-Sanchez, T. Ahmido, D. Casimir, S. Baliga and P. Misra, *J. Phys. Chem. A*, 2013, **117**, 13825−13831.

28 S. Bai, K. Zhang, L. Wang, J. Sun, R. Luo, D. Li and A. Chen, *J. Mater. Chem. A*, 2014, **2**, 7927-7934.

29 L. M. Bertus, C. Faure, A. Danine, C. Labrugere, G. Campet, A. Rougier and A. Duta, *Mater. Chem. Phys.*, 2013, **140**, 49-59.

30 M. Aslam, M. T. Qamar, M. T. Soomro, I. M. I. Ismail, N. Salah, T. Almeelbi, M. A. Gondal and A. Hameed, *Appl. Catal., B*, 2016, **180**, 391–402.

31 Z. Jiao, J. Wang, L. Ke, X. W. Sun and H. V. Demir, *ACS Appl. Mater. Interfaces* 2011, **3,** 229-236.

32 L. Feng, D. T. Hoang, C. K. Tsung, W. Huang, S. H. -Y. Lo, J. B. Wood, H. Wang, J. Tang and P. Yang, *Nano Res.,* 2011, **4,** 61–71.

33 M. Aslam, M. T. Soomro, I. M. I. Ismail, N. Salah, M. W. Ashraf, H. A. Qari and A. Hameed, *Arabian J. Chem.*, 2015, *http://dx.doi.org/10.1016/j.arabjc.2015.05.001*

34 M. H. Priya and G. Madras, *Ind. Eng. Chem. Res.* 2006, **45,** 482-486.

Figure captions

Fig. 1. (a) The comparison of the solid-state absorption spectra (b) the graphical evaluation of the bandgaps of pure, 1% and 5 Ce^{3+} impregnated WO_3 whereas the bandgap evaluation for 10%, 15%, 20% and 25% Ce^{3+} impregnated WO_3 is presented in the inset of (b). The inset of (a) shows the exploded view of the spectra in 450-700 nm range.

Fig. 2. The comparison of the (a) PL spectra (b) Raman spectra of pure, 1%, 5%, 10%, 15%, 20% and 25% Ce^{3+} impregnated WO_3. The inset of (b) shows the exploded view of the Raman spectra from 750-850 cm^{-1}.

Fig. 3. The comparison of the XRD patterns of pure, 1%, 5%, 10%, 15%, 20% and 25% Ce^{3+} impregnated WO_3. The reflections due to Ce^{3+} are marked by arrows. The inset presents the growth of reflections in the 2θ range of 35.6^o-40.6^o due to Ce^{3+} impregnation.

Fig. 4. The XPS analysis of 10% Ce^{3+} impregnated WO_3 (a) The survey scan in the binding energy range of 0 to 1100 eV (b) W4f splitted levels (c) Ce3d splitted levels and (d) O1s.

Fig. 5. The comparison of the FESEM images of pure (a) WO_3, (b) 5%, (c) 10%, (d) 15%, (e) 20% and (f) 25% Ce^{3+} impregnated WO_3 at the resolution of 200,000×.

Fig. 6. The comparison of EDX spectra of pure, 5%, 10% and 20% Ce^{3+} loaded WO_3.

Fig. 7. The typical HRTEM image of 5% Ce^{3+} loaded WO_3 (a) at 20 nm (b) at 10 nm (c) image of red marked area in (b) at 1 nm (d) image of orange marked area in (b) at 2 nm. The (e) and (f) are the line scans of (c) and (d) showing a d-spacing of 0.33 nm and 0.35 nm.

Fig. 8. The comparison of charge discharge profiles of (a) pure (b) 1% (c) 5% (d) 10% (e) 15% and (f) 20% Ce^{3+} loaded WO_3 in the dark and under illumination. The three cycles were recorded at 0, 5 and 10 min.

Fig. 9. The comparison of the performance of pure, 1%, 5%, 10%, 15%, 20% and 25% Ce^{3+} impregnated WO_3 (50mg/150 ml) for the degradation of (a) 2-NP (50 ppm) and (c) 2-CP (50 ppm) in the sunlight exposure ($1100\pm100 \times 10^2$ lx). The plots of $\ln(C_o/C)$ versus sunlight exposure time are shown in (b)2-NP and (d) 2-CP.

Fig. 10. The comparison of the performance of pure, 1%, 5%, 10%, 15%, 20% and 25% Ce^{3+} impregnated WO_3 (50 mg each per 150 ml) for the mineralization of (a) 2-NP and (b) 2-CP (50 ppm each) in the sunlight exposure ($1100\pm100 \times 10^2$ lx).

Fig. 11. The time scale IC profiles for the release of ions during the degradation of (a) 2-NP and (b) 2-CP in sunlight exposure over 20% Ce^{3+} impregnated WO_3.

Fig. 12. The performance evaluation of 20% Ce^{3+} impregnated WO_3 for five consecutive cycles.

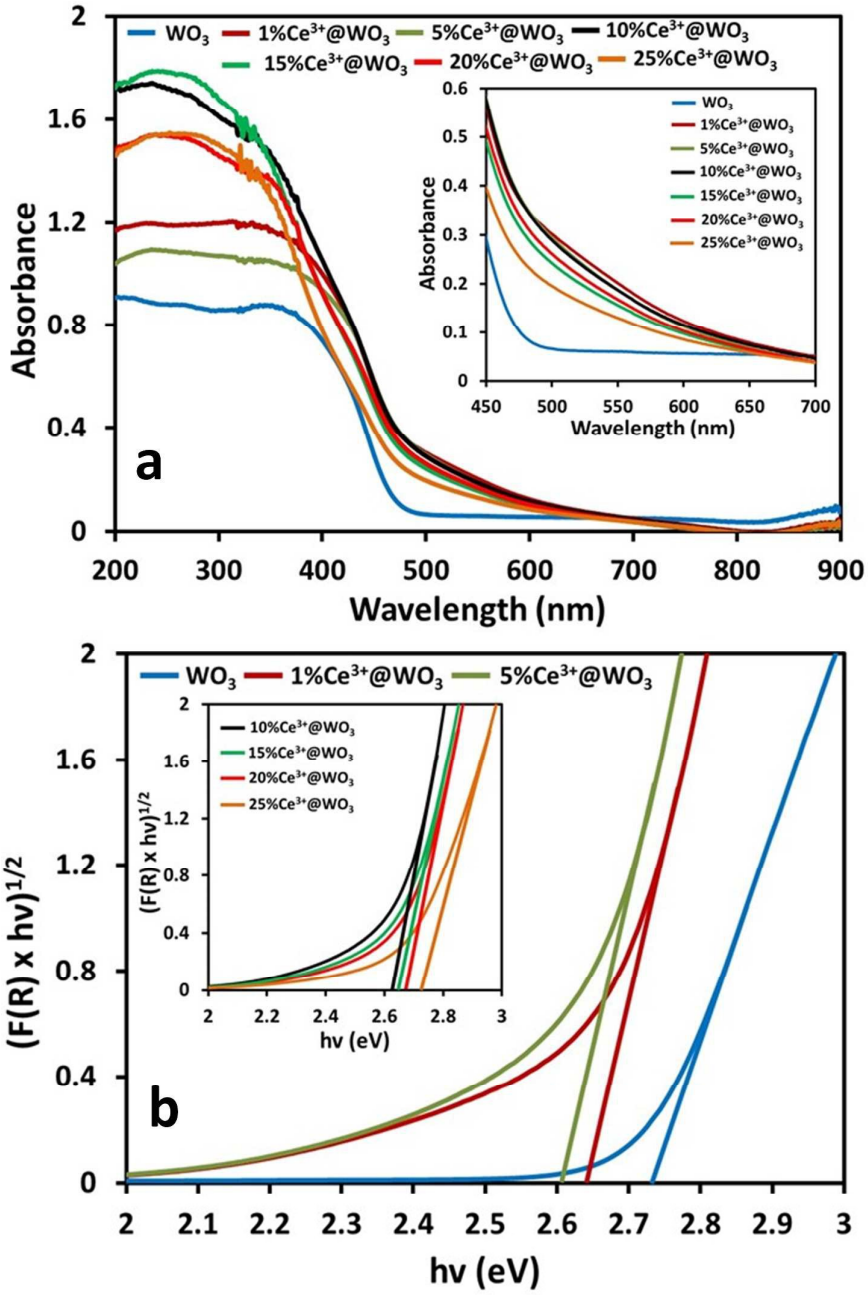

Fig. 1. (a) The comparison of the solid-state absorption spectra (b) the graphical evaluation of the bandgaps of pure, 1% and 5% Ce^{3+} impregnated WO_3 whereas the bandgap evaluation for 10%, 15%, 20% and 25% Ce^{3+} impregnated WO_3 is presented in the inset of (b). The inset of (a) shows the exploded view of the spectra in 450-700 nm range.

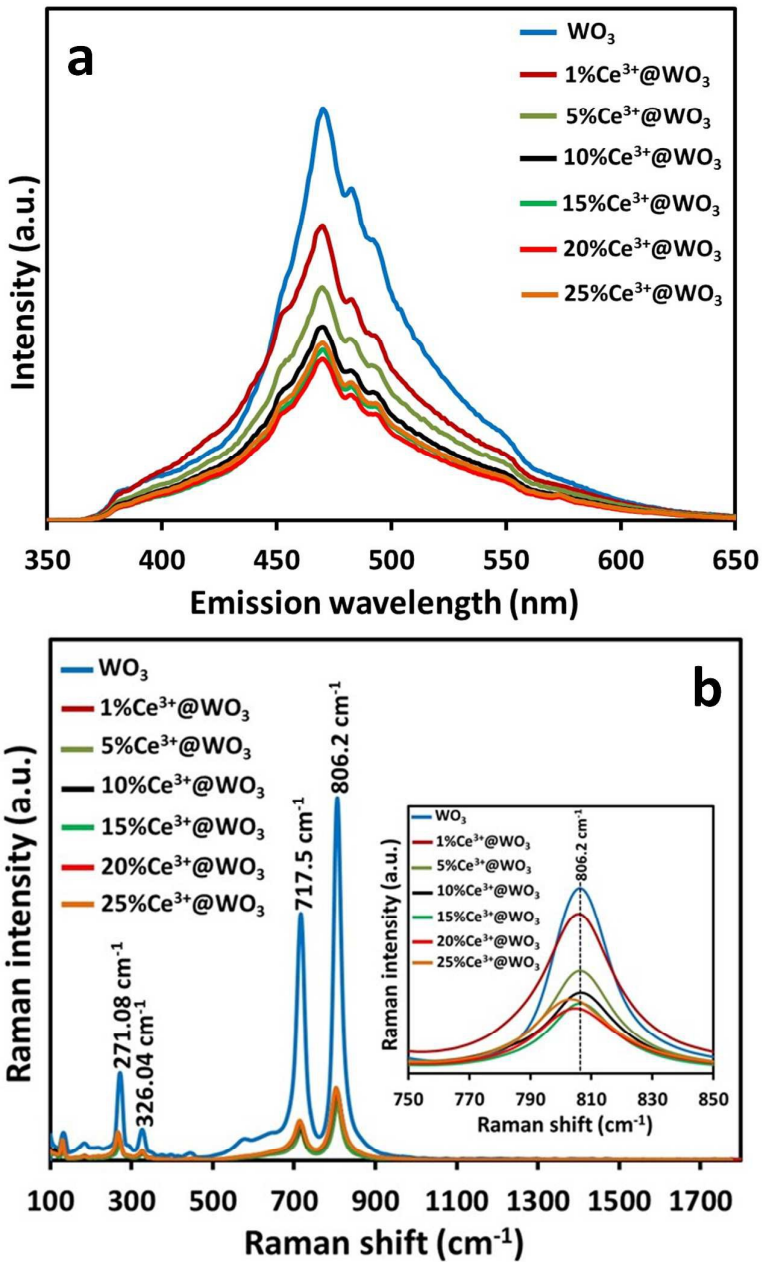

Fig. 2. The comparison of the (a) PL spectra (b) Raman spectra of pure, 1%, 5%, 10%, 15%, 20% and 25% Ce^{3+} impregnated WO_3. The inset of (b) shows the exploded view of the Raman spectra from 750-850 cm^{-1}.

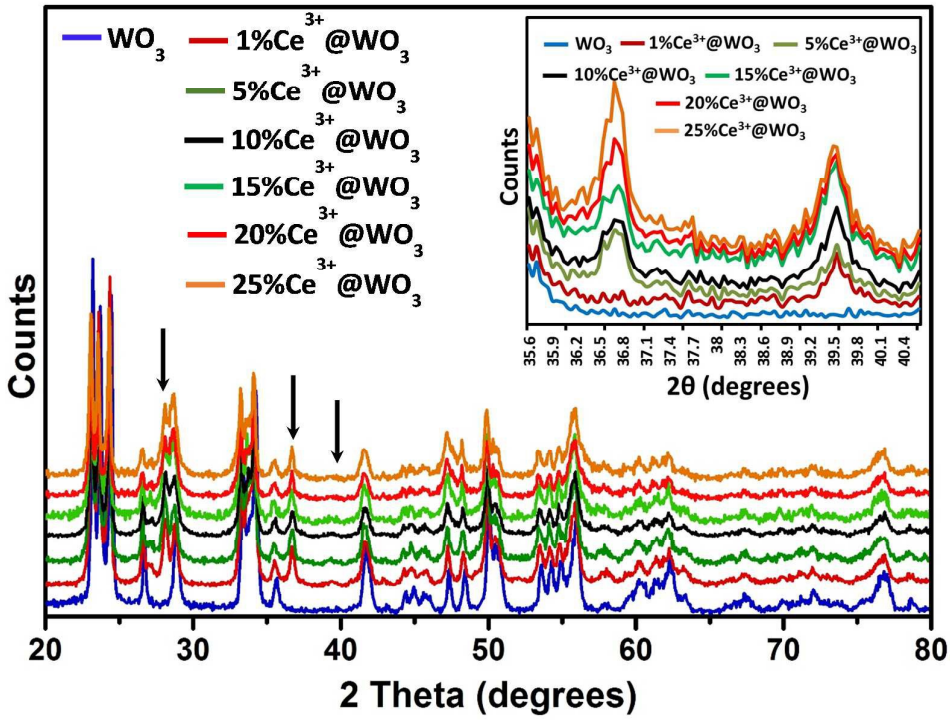

Fig. 3. The comparison of the XRD patterns of pure, 1%, 5%, 10%, 15%, 20% and 25% Ce^{3+} impregnated WO_3. The reflections due to Ce^{3+} are marked by arrows. The inset presents the growth of reflections in the 2θ range of 35.6°-40.6° due to Ce^{3+} impregnation.

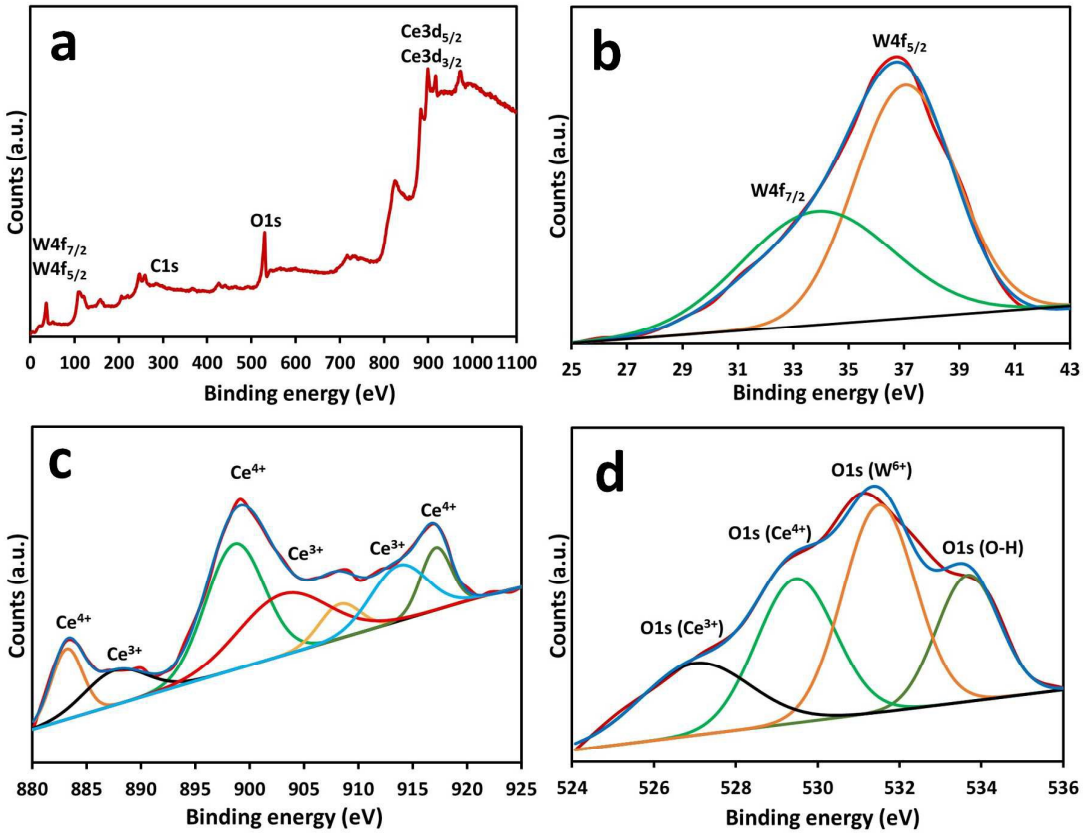

Fig. 4. The XPS analysis of 10% Ce^{3+} impregnated WO_3 (a) The survey scan in the binding energy range of 0 to 1100 eV (b) W4f splitted levels (c) Ce3d splitted levels and (d) O1s.

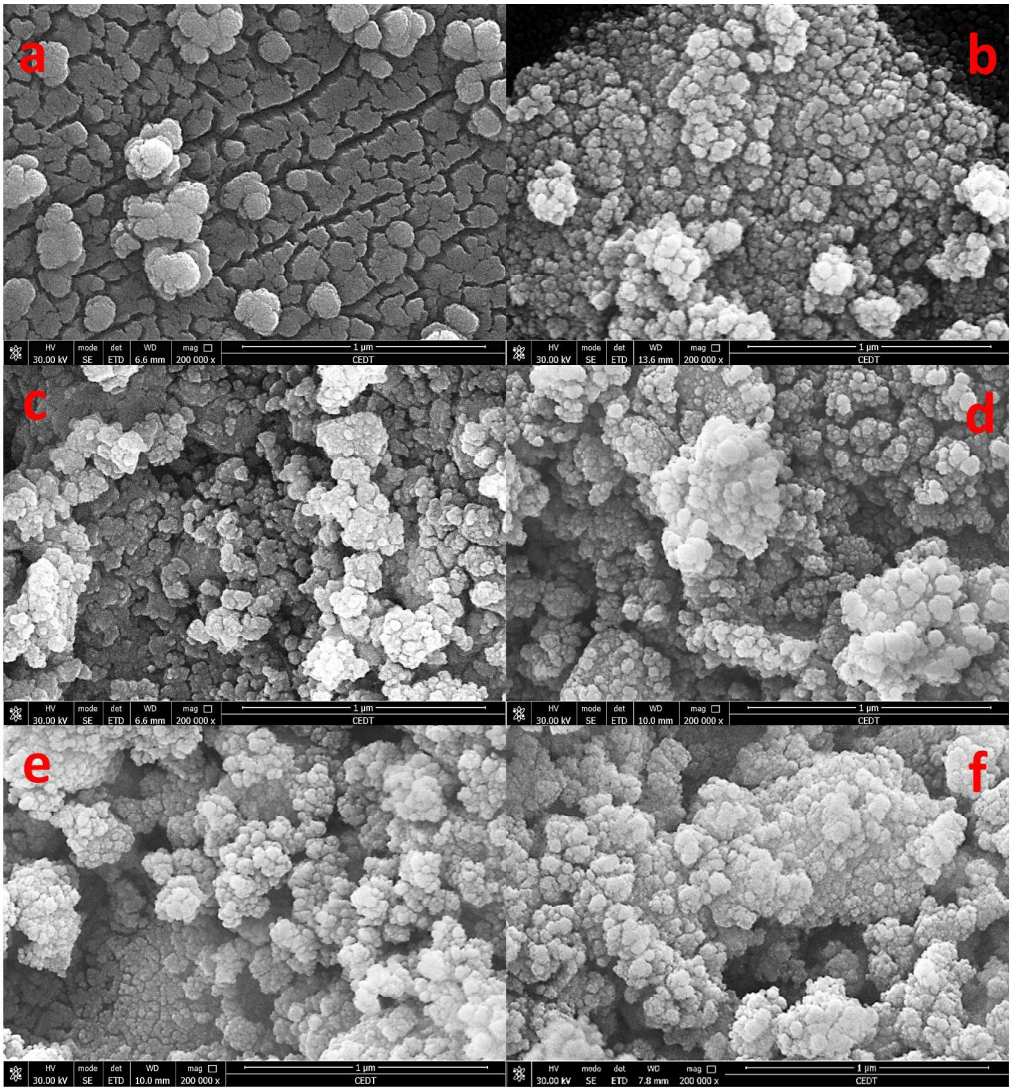

Fig. 5. The comparison of the FESEM images of pure (a) WO_3, (b) 5%, (c) 10%, (d) 15%, (e) 20% and (f) 25% Ce^{3+} impregnated WO_3 at the resolution of 200,000×.

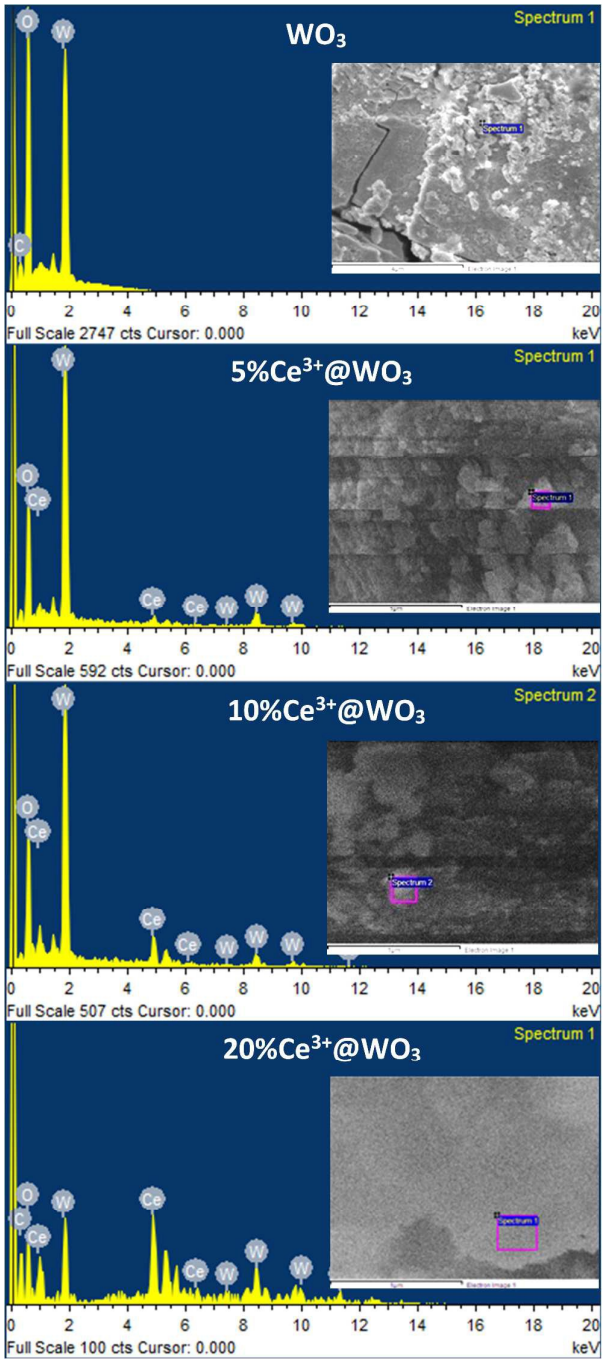

Fig. 6. The comparison of EDX spectra of pure, 5%, 10% and 20% Ce^{3+} loaded WO_3.

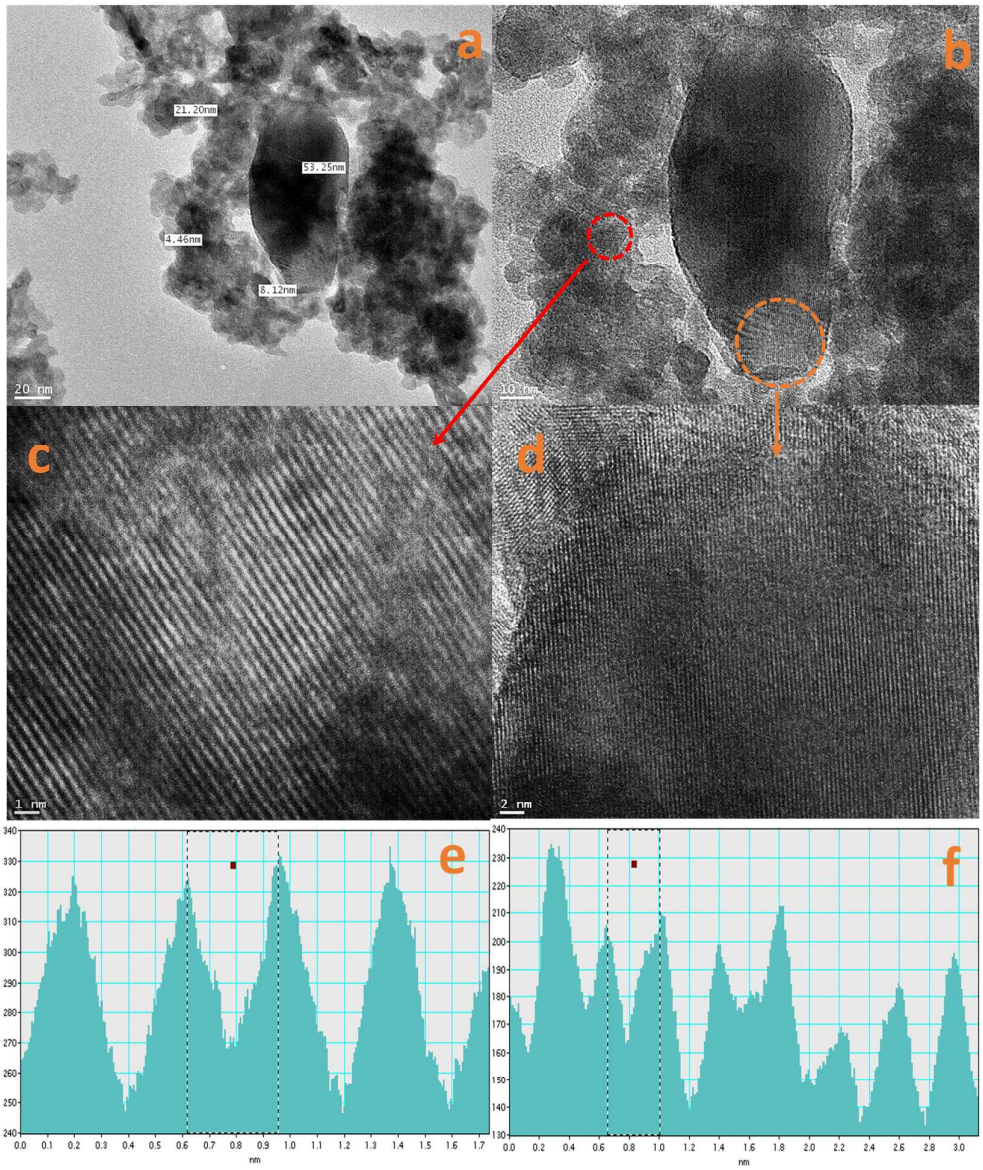

Fig. 7. The typical HRTEM image of 5% Ce^{3+} loaded WO_3 (a) at 20 nm (b) at 10 nm (c) image of red marked area in (b) at 1 nm (d) image of orange marked area in (b) at 2 nm. The (e) and (f) are the line scans of (c) and (d) showing a d-spacing of 0.33 nm and 0.35 nm.

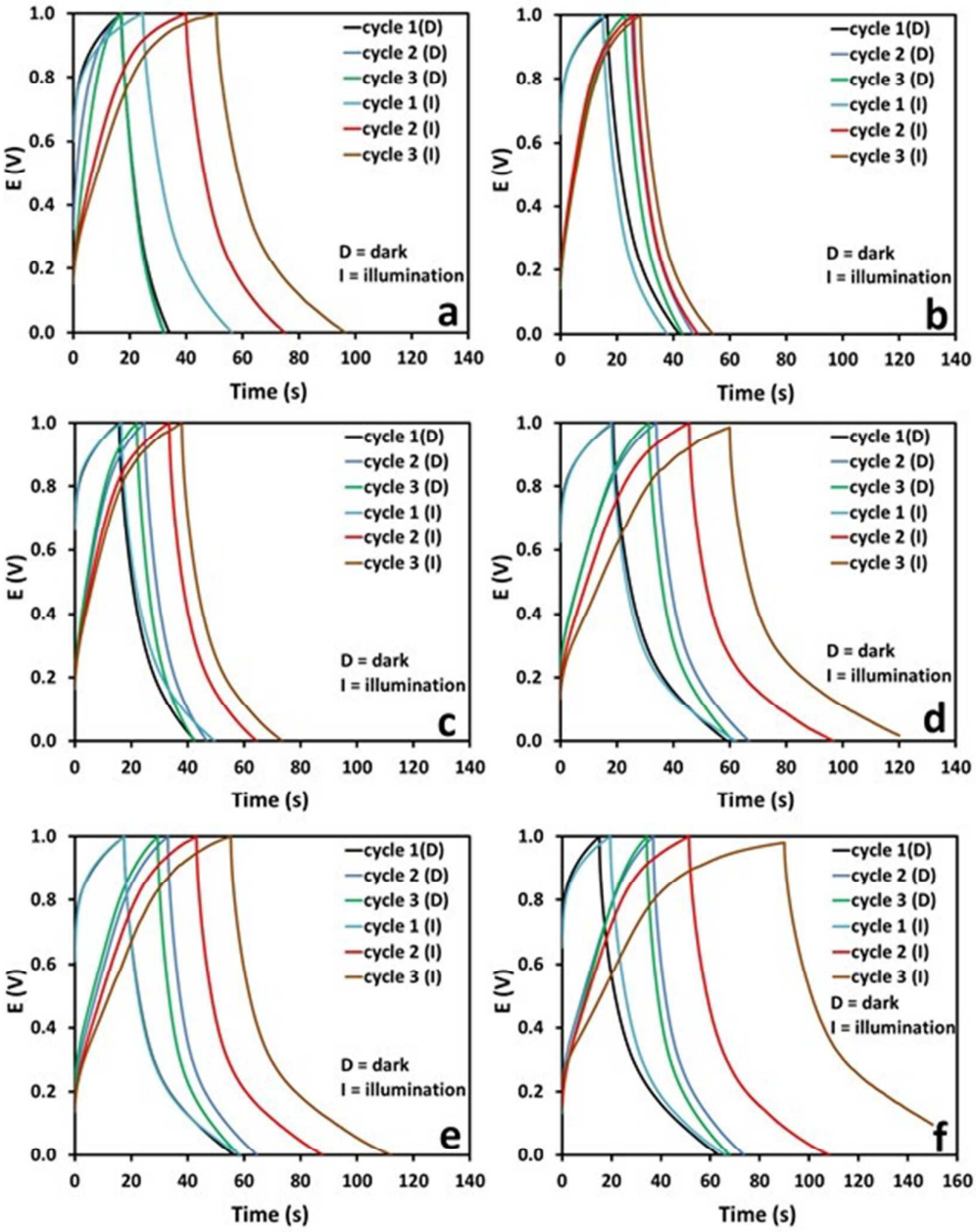

Fig. 8. The comparison of charge discharge profiles of (a) pure (b) 1% (c) 5% (d) 10% (e) 15% and (f) 20% Ce^{3+} loaded WO_3 in the dark and under illumination. The three cycles were recorded at 0, 5 and 10 min.

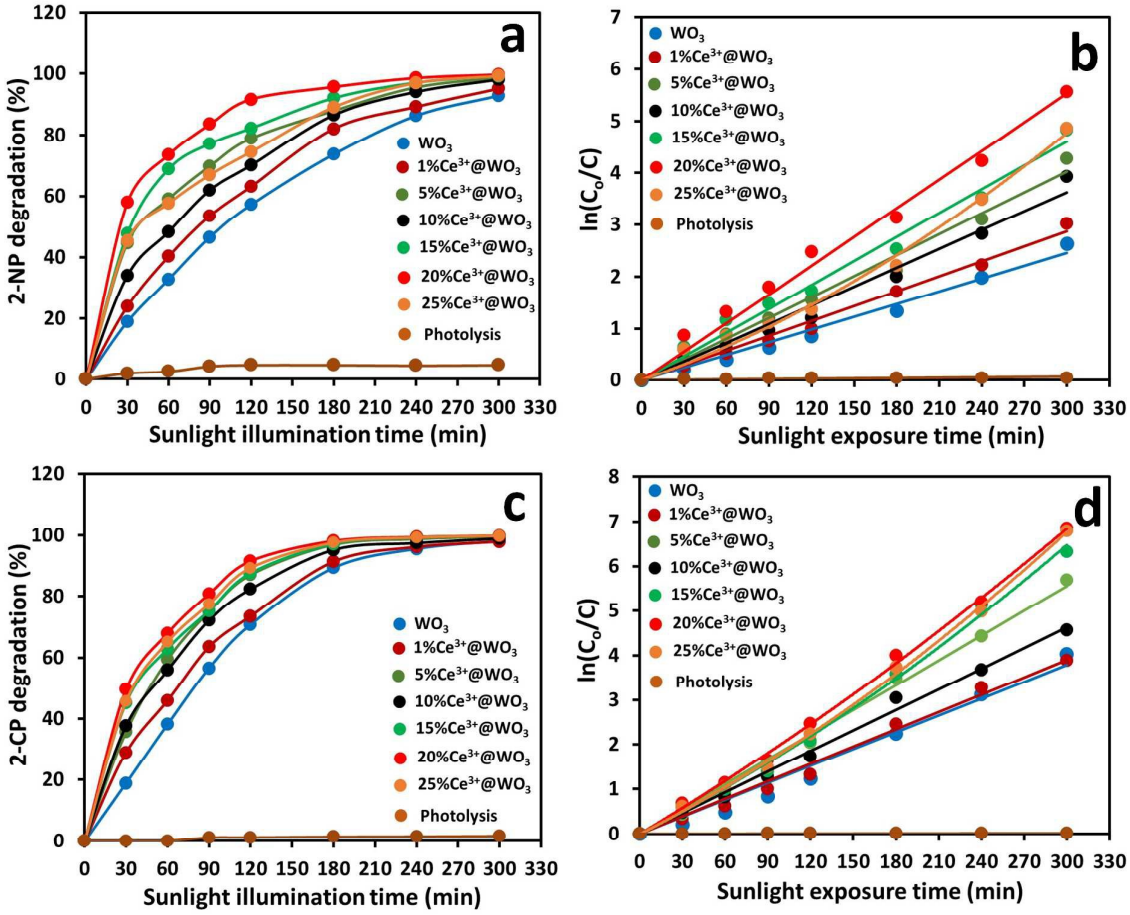

Fig. 9. The comparison of the performance of pure, 1%, 5%, 10%, 15%, 20% and 25% Ce^{3+} impregnated WO_3 (50mg/150 ml) for the degradation of (a) 2-NP (50 ppm) and (c) 2-CP (50 ppm) in the sunlight exposure (1100±100 × 10^2 lx). The plots of $ln(C_o/C)$ versus sunlight exposure time are shown in (b) 2-NP and (d) 2CP.

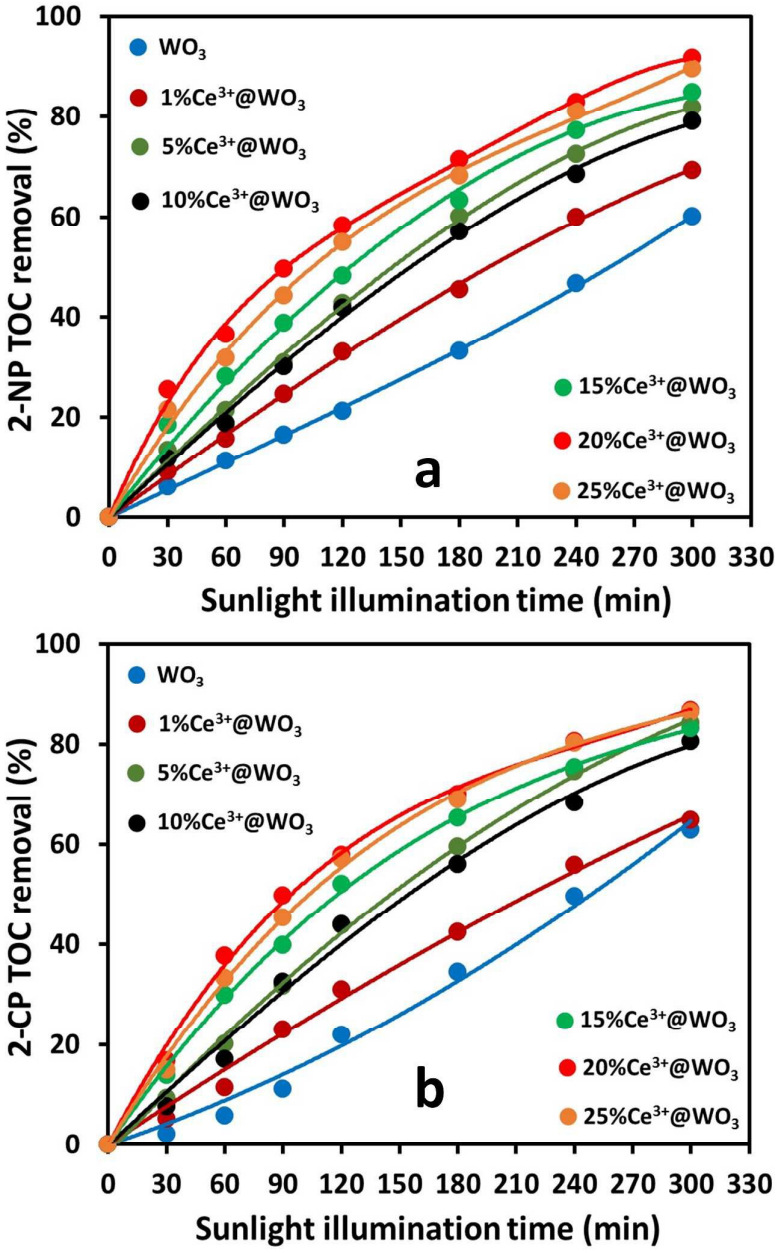

Fig. 10. The comparison of the performance of pure, 1%, 5%, 10%, 15%, 20% and 25% Ce^{3+} impregnated WO_3 (50 mg each per 150 ml) for the mineralization of (a) 2-NP and (b) 2-CP (50 ppm each) in the sunlight exposure ($1100\pm100 \times 10^2$ lx).

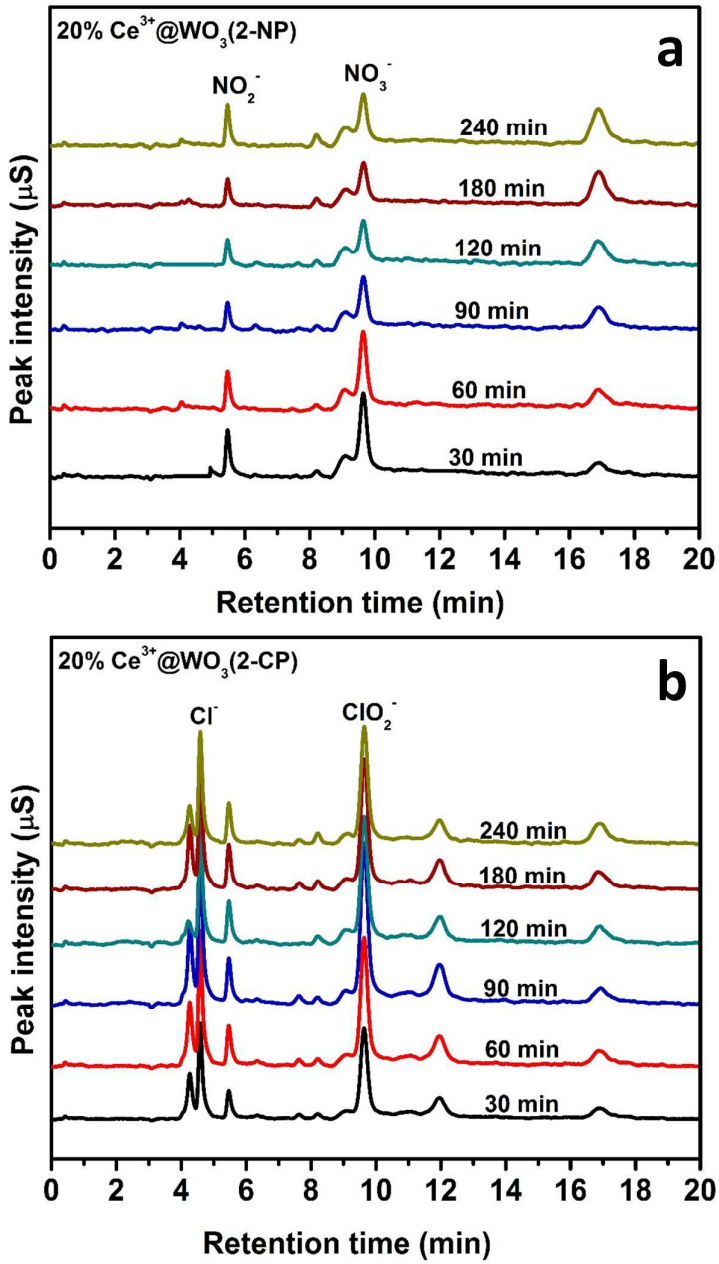

Fig. 11. The time scale IC profiles for the release of ions during the degradation of (a) 2-NP and (b) 2-CP in sunlight exposure over 20% Ce^{3+} impregnated WO_3.

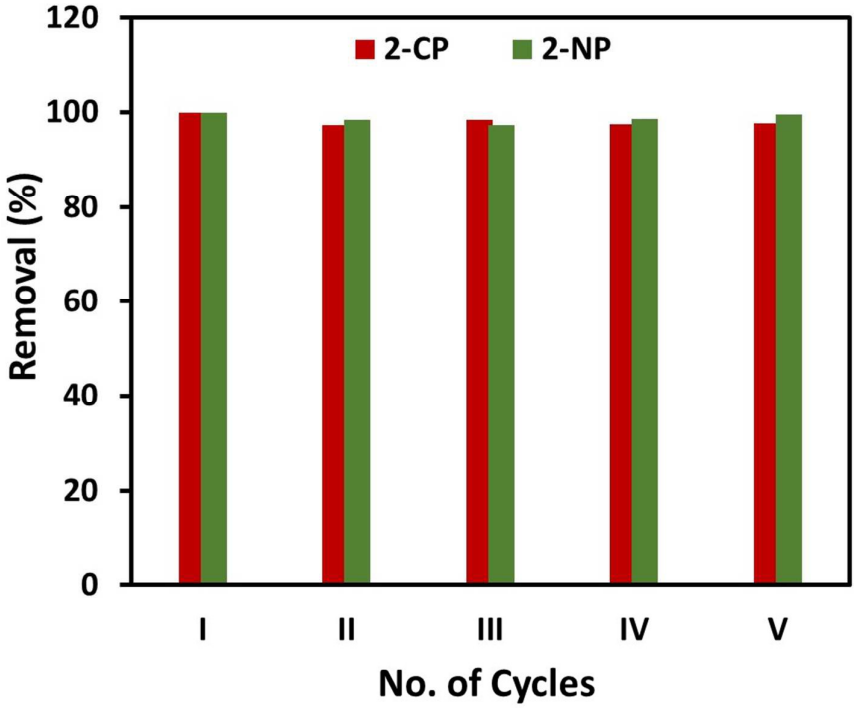

Fig. 12. The performance evaluation of 20% Ce^{3+} impregnated WO_3 for five consecutive cycles.

Graphical Abstract